Journal of Theoretical Biology 374 (2015) 26–34

Contents lists available at ScienceDirect

Journal of Theoretical Biology

journal homepage: www.elsevier.com/locate/yjtbi

"Cargo-mooring" as an operating principle for molecular motors

Bartosz Lisowski [a,b,*], Łukasz Kuśmierz [a,c], Michał Żabicki [a], Martin Bier [d]

[a] M. Smoluchowski Institute of Physics Jagiellonian University, Kraków, Poland
[b] Unit of Pharmacoepidemiology and Pharmacoeconomics, Faculty of Pharmacy, Jagiellonian University Medical College, Kraków, Poland
[c] AGH University of Science and Technology, Institute of Automatics, Al. Mickiewicza 30, 30-059, Krakow, Poland
[d] Department of Physics, East Carolina University, Greenville, NC 27858, USA

HIGHLIGHTS

- Experiments suggest that cargo dynamics play a role for kinesin's motion.
- We work out how chemical energy can be used to rectify the cargo's diffusion.
- Kinesin and its cargo interact cooperatively to move along the polymeric track.
- We derive the velocity as a function of load force, cargo size and buffer viscosity.
- Experimental observations appear consistent with our results.

ARTICLE INFO

Article history:
Received 20 August 2014
Received in revised form
26 January 2015
Accepted 4 March 2015
Available online 17 March 2015

PACS:
87.10.-e
87.18.-h
87.16.Nn
87.15.Vv

Keywords:
Kinesin
Molecular motors
Diffusion
Intracellular transport

ABSTRACT

Navigating through an ever-changing and unsteady environment, and utilizing chemical energy, molecular motors transport the cell's crucial components, such as organelles and vesicles filled with neurotransmitter. They generate force and pull cargo, as they literally walk along the polymeric tracks, e.g. microtubules.

What we suggest in this paper is that the motor protein is not really pulling its load. The load is subject to diffusion and the motor may be doing little else than rectifying the fluctuations, i.e. ratcheting the load's diffusion. Below we present a detailed model to show how such ratcheting can quantitatively account for observed data.

The consequence of such a mechanism is the dependence of the transport's speed and efficacy not only on the motor, but also on the cargo (especially its size) and on the environment (i.e. its viscosity and structure). Current experimental works rarely provide this type of information for *in vivo* studies. We suggest that even small differences between assays can impact the outcome. Our results agree with those obtained in wet laboratories and provide novel insight in a molecular motor's functioning.

1. Introduction

For eukaryotic cells, free diffusion is simply too slow and too uncontrollable to take care of the transport needs. For this reason the motion of certain vesicles and organelles involves motor proteins and their filamentous tracks. This guarantees proper cell functioning. Intracellular active transport is something that every eukaryotic cell has to coordinate, maintain and constantly shape. It involves many players, like different types of filaments, molecular motors and cargos that are moved from one place to another. Many of these components can be studied in isolation *in vitro*. Milestone works on kinesin-1, experimental (Svoboda et al., 1993; Visscher et al., 1999; Howard, 1997) as well as theoretical (Astumian and Bier, 1994; Astumian, 1997; Jülicher et al., 1997), have brought many scientists from different fields to the topic of active intracellular transport. A lot of questions have been both asked and answered. We now know for instance that the *walking* pattern is "hand-over-hand" and not "inchworm" (Asbury, 2003; Yildiz et al., 2004). Also the role of the neck linker that connects the two heads has been cleared up to a large extent (Guydosh and Block, 2006; Kozielski et al., 1997; Tomishige et al., 2006; Mogilner et al., 2001; Shastry and Hancock, 2011). We have, furthermore, attained a good understanding of the relation between mechanics and chemistry (Mori et al., 2007).

But there are still unsolved problems.

The moving motor protein uses chemical energy to overcome the viscous friction of the cytosol and to drive the conformational

* Corresponding author.
E-mail address: bartek.lisowski@uj.edu.pl (B. Lisowski).

http://dx.doi.org/10.1016/j.jtbi.2015.03.007
0022-5193/

changes in the catalytic cycle. In experiments it is possible to apply an external load with an optical tweezer: an external load that the motor has to also work against.

The most efficient way of transporting cargo in a viscous medium would be pulling it with constant velocity from the place where it is formed to its destination. It would lead to trajectories with position linearly dependent on time. However, the "staircase"-like trajectories as obtained experimentally (e.g. as in Svoboda et al., 1993) exclude such a mechanism of smooth active transport. Instead, the experimental results suggest that the cargo is displaced in rapid "jerks". Those jerks correspond to single steps of the molecular motor that transports the cargo. The energy needed for this can be estimated. It is apparent that evolution lead to a mechanism that is not the most efficient in terms of energy (see Section 1 in **SI**).

Experimentalists have found that the stalk (the relatively long construct between the heads and the cargo) plays a role in triggering kinesin's steps (Dietrich et al., 2008; Wong et al., 2009; Yildiz et al., 2008). It appears that kinesin's heads "communicate" with the cargo through the stalk. New structural data on molecular motors are rapidly becoming available. Many of the more phenomenological models focus on enzymatic activity and describe rather than explain the force generation. Below we present a model where the force generation is a result of the motor rectifying the cargo's fluctuations. The communication necessary for such an "information ratchet" is exchanged through the stalk.

In the model we propose that the molecular motor works as a mooring rope which sequentially changes the docking point – thus walking along its track. As our foremost reference we use kinesin-1. Obtained results agree with experimental data and the construction of the presented model allows for a new insight into the functioning of motor proteins.

2. Model

We consider a system consisting of a motor carrying a spherical cargo along a polymeric track, see Fig. 1A. All the components are embedded in a buffer solution of a known viscosity. The track has a periodic structure, with special domains — binding sites — positioned every $L=8$ nm. This corresponds to the known molecular structure of microtubule (Howard, 2001). The cargo — e.g. a spherical vesicle or a bead of radius R — is subject to diffusion in the surrounding solution. It is attached to the motor, which in turn holds on to the binding site, hence it may move only within a limited range, $2x_m$ (Fig. 1B). This range is determined by the length and elasticity of the cargo–motor connection. Later in this section we consider the case of $x_m = L$.

Somewhat like a windswept balloon on a string, the Brownian motion of the cargo makes the motor swing back and forth around the docking point. The deflection, however, will not exceed the maximum value, $\phi_{\max}$ (cf. Fig. 1). Again, this limit is determined by the structural properties (e.g. elasticity) of the setup.

In what follows we will examine the system in terms of the relative position, x_{rel}, between only two points, $x_{rel} = x_{top} - x_{bottom}$. The position of the top point, x_{top}, represents the position of the cargo which we assume to be the same as the position of the motor–cargo link and the cargo's center. The top point can move to the left and to the right due to thermal diffusion in a continuous range. The position of the bottom point, x_{bottom}, represents the position of the midpoint between motor's two heads. It can change by L only via discrete steps from one binding site to a next one. In what comes next we also assume that the motor is fully processive. This means that it never detaches from the track.

The stepping process is coupled to a sequence of a chemical reactions. For kinesin-1, as well as for other cytoskeletal motor proteins, this would be the hydrolysis of ATP. Here we do not consider

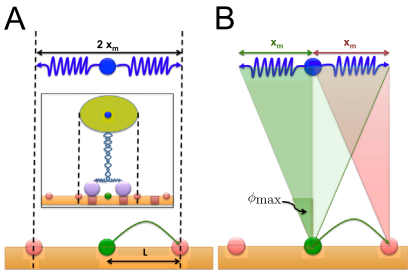

Fig. 1. *Cartoon presenting the model's idea.* (A) The motor is described through the behavior of two points. The top one (blue) represents the cargo. It moves in the continuous range $2x_m$, driven by Brownian motion. The bottom one (green) stands for the position of the motor on a track (orange). Each step of a motor is a discrete jump of length L between two neighboring binding sites (red circles). The top point reflects the position of the cargo, while the bottom point reflects the position of the midpoint between the two docked heads. The inset in A shows the ideogram of a kinesin-like motor. It consists of two heads (here in violet), connected with spring-like neck linkers, which later intertwine to form a stalk (blue wiggly lines). The top of the stalk connects with the cargo (yellow oval). The motor walks on a microtubule (orange). Note that the real microtubule's binding sites (red squares) are shifted by 4 nm relative to the modeled ones (red circles). (B) A step may occur when the position of the cargo allows for it. After jumping from one binding site to the other (e.g. from green to red, as depicted by the green arrow), the angle between the upper and the lower point must be no larger than the maximal deflection ϕ_{max} (reddish for the red binding site). (For interpretation of the references to color in this figure caption, the reader is referred to the web version of this paper.)

those reactions in detail. For these reactions the motor takes substrates from the buffer solution and acts like an enzyme for the conversion of this substrate into a lower-energy product. The chemical reactions trigger conformational changes of the motor. They let the bottom point detach from the previously occupied site and reattach at the neighboring one. The chemical cycle is evidently not an instantaneous process. It takes t_r to complete the cycle and so no step is possible in a time shorter than t_r. However, finishing the cycle is not sufficient for the motor to make a step.

After finishing the chemical cycle *and* when the position of the cargo allows it, the motor changes its docking point, i.e. takes an $L=8$ nm jump to the right. Assume that the motor is deflected by $\phi_{\max}$ to the left, so that $x_{rel} = -L$ (Fig. 1B). The architecture of the microtubule–kinesin–cargo system implies steric constraints that will not permit the cargo to further diffuse to the left. These constraints effectively set up a reflecting barrier for the diffusing cargo. Eventually diffusion will bring the cargo to $x_{rel} \geq 0$. Then a next step will occur provided that the chemical cycle is also completed.

Imagine that only the first condition (completion of all chemical transitions) has been fulfilled and the relative position between the top and the bottom point stays in the range $-L \leq x_{rel} < 0$. If the motor would make a step and increase the position of the bottom point by L without any change in the position of the top point (since the motor does not pull the cargo), then it would have to deflect by an angle greater than $\phi_{\max}$ to the left. This is impossible due to structural limitations.

The motion is conceived as taking place in one dimension. Natural kinesin-1 walks straight along the microtubule and does not wander to the left or right. The cargo however may diffuse sideways. The reason for our 1-dimensional idealization is that the 2-dimensional optical trap methods revealed that sideways loads exerted on the cargo do not significantly affect the directed motion of the motor (Block et al., 2003). This is in contrast with the motor's high sensitivity for longitudinal loads. If there is any communication between the cargo and the motor, it should be captured by our 1-dimensional approximation.

For simplicity, we first present the derivation without considering backsteps, i.e., without steps back to the binding site on the left (cf. Fig. 1). Then, in the section "Backstepping," we show how to broaden the analysis and take backsteps into account.

Table 1
Variables used in the derivation of the force–velocity relation.

x_m	Half-length of the load's diffusion interval
L	Step size
D	Diffusion coefficient of the cargo
t_r	Time of an unloaded kinesin's chemical reactions which lead to a mechanical step
F	Load force, as the motor is stepping from left to right; F is pulling to the left if $F>0$ and to the right if $F<0$
γ	Drag coefficient
$z=F/(\gamma D)$	

2.1. Analytical description

In our model the cargo is positioned at a fixed distance from the track and executing diffusive motion parallel to the track. We take $x \equiv x_{\top}$ for the position of the cargo along the direction of the track. Table 1 lists all the symbols used in this and further sections. The evolution in time of the probability density distribution for x is described by a Fokker–Planck–Smoluchowski equation:

$$\partial_t p(x,t\,|\,x_0,0) = \frac{F}{\gamma}\partial_x p(x,t\,|\,x_0,0) + D\partial_{xx}^2 p(x,t\,|\,x_0,0). \tag{1}$$

Here the first term on the right hand side describes the forward drift coming from the optical trap, which holds on to the cargo and applies a load force F. The second term describes the diffusive spreading. The drag coefficient, $\gamma = 6\pi\eta R$ (R is the radius of the cargo and η is the viscosity of the solution), and the diffusion coefficient, D, are connected through the fluctuation–dissipation theorem, $D = k_B T/\gamma$.

We split the motor's step into two stages. During the first stage the load diffuses in the range $(-x_m, x_m)$ with reflecting boundary conditions. No mechanical step can be made during this stage. After the time t_r the motor is able to make a step if no geometrical obstacles prevent it. For our model it means that positions of cargo and motor fulfill a condition $x > -x_m + L$. We assume that during the second stage the motor makes a step immediately upon fulfilling the geometrical condition. After t_r we thus have the same Fokker–Planck–Smoluchowski equation, but with different boundary conditions. While the left boundary is still reflecting, the right boundary becomes absorbing. We are particularly interested in the mean time needed for the cargo to cross the latter boundary. This will trigger the motor to make one mechanical step: the rear head of the motor will detach from the microtubule and dock at the binding site in front of the leading head, $2L$ ahead of its original position. The motion of the rear head is in general a combination of diffusion and directed motion, but with a lot of subtleties (Block, 2007).

Our aim is to find force–velocity relations, that is to examine how the external force brought about by the optical tweezer affects the dynamics of the motor. We note that the correct way of measuring the motor's velocity is through $v = L/\langle t_{step}\rangle$. In Section 2 of the **SI** it is shown how and why $v = L\langle 1/t_{step}\rangle$ leads to wrong results.

2.1.1. Derivation

For t_r larger than the timescale of the Brownian jerks, we may write

$$p(x, t_r\,|\,x_0, 0) \approx p_s(x), \tag{2}$$

where $p_s(x)$ stands for the stationary distribution of the cargo's position for the first stage. As mentioned before, we impose reflecting boundary conditions and obtain a current:

$$j_s(x_m) = -\frac{F}{\gamma}p_s(x_m) - D\partial_x p_s(x_m) = 0 = j_s(-x_m). \tag{3}$$

From this and from the normalization condition of the probability density function on the interval $(-x_m, x_m)$, an explicit formula for the stationary probability distribution can be obtained. It is an ordinary exponential distribution:

$$p_s(x) = \frac{z e^{-zx}}{2\sinh z x_m}, \tag{4}$$

where $z \equiv F/(\gamma D)$.

If after the first stage $x > -x_m + L$, then the step can be made immediately. Let p_1 denote the probability of this event:

$$p_1 = \int_{-x_m+L}^{x_m} \mathrm{d}x\, p_s(x) = \frac{e^{z(x_m-L)} - e^{-zx_m}}{2\sinh z x_m}. \tag{5}$$

We will denote by p_0 the probability of the complementary event, i.e. the event in which the motor cannot make a step because of geometrical constraints ($x + x_m > L$ is then a condition *sine qua non* for a step to be possible):

$$p_0 = \int_{-x_m}^{-x_m+L} \mathrm{d}x\, p_s(x) = \frac{e^{zx_m}}{2\sinh z x_m}(1 - e^{-zL}). \tag{6}$$

The last element we need is a mean first passage time (MFPT). If the cargo is in the interval $(-x_m, -x_m + L)$, then the motor has to wait until the cargo will reach the right (absorbing) boundary. We therefore analyze the same system with different boundary and initial conditions. Notice that we shift the interval by x_m to the right. This will simplify the final formulas:

$$\begin{cases} j(0,t) &= -\dfrac{F}{\gamma}p(0,t) - D(\partial_x p)(0,t) = 0 \\ p(L,t) &= 0 \\ p(x,0) &= P(X = x - x_m\,|\,-x_m < X < -x_m + L) \\ &= \dfrac{p_s(x - x_m)}{p_0}. \end{cases} \tag{7}$$

In order to obtain the MFPT we use the formula from the standard textbook by Gardiner (1997, Chapter 5, Section 5.2.7, Eq. (5.2.160)):

$$\langle t_{fp}\,|\,x\rangle = \frac{1}{D}\int_x^L \mathrm{d}u\, e^{zu}\int_0^u \mathrm{d}y\, e^{-zy} = \frac{1}{zD}\left(\frac{1}{z}(e^{zL} - e^{zx}) - (L - x)\right), \tag{8}$$

where x denotes the starting position. Now we have to average over the distribution (cf. Eq. (4)) that constitutes our initial condition:

$$\langle t_{fp}\rangle = \int_0^L \mathrm{d}x\, \langle t_{fp}\,|\,x\rangle p(x,0). \tag{9}$$

Having done this, we are ready to write down for the mean step time:

$$\langle t_{step}\rangle = p_1 t_r + p_0(t_r + \langle t_{fp}\rangle) = t_r + \int_0^L \mathrm{d}x\, \langle t_{fp}\,|\,x\rangle p_s(x - x_m). \tag{10}$$

The result reads as follows:

$$\langle t_{step}\rangle = t_r + \frac{e^{zx_m}}{\dfrac{F}{\gamma} z \sinh z x_m}(\sinh zL - zL). \tag{11}$$

With $v = L/\langle t_{step}\rangle$ the resulting force–velocity curve is found to be given by the formula:

$$v = \frac{L\frac{F}{\gamma} z \sinh zx_m}{t_r \frac{F}{\gamma} z \sinh zx_m + e^{zx_m}(\sinh zL - zL)}. \quad (12)$$

The important limits are easily derived:

$$\lim_{F\to\infty} v = 0,$$
$$\lim_{F\to-\infty} v = \frac{L}{t_r},$$
$$\lim_{F\to 0} v = \frac{L}{t_r + \frac{L^3}{6Dx_m}}. \quad (13)$$

We note that it is possible to derive simplified approximations of force–velocity relations for a kinesin-like motor using the approach proposed by Bier et al. (1999). However, Eq. (12) originates directly from the model's assumptions and is therefore presented in its full form.

3. Results

In a typical *in vitro* experiment we have kinesins walking along microtubule and carrying a small silica bead. The bead is trapped in the narrow laser of the optical tweezer. How can this force, acting on a bead, be transferred through the long (ca. 110 nm) stalk and neck linkers to the motor domain of the kinesin heads? How can it be that this force interferes with the reaction rates, changing their values by a factor of $\exp[FL/(k_BT)]$? While we know quite a lot about, for instance, the importance of strain gating (Guydosh and Block, 2006) for a head's coordination, it is much more challenging to describe how the information about load reaches the binding sites of motor domains. While the chemomechanical approach towards modeling motor proteins (Liepelt and Lipowsky, 2007; Clancy et al., 2011; Fisher and Kolomeisky, 1999; Schilstra and Martin, 2006) explains the impact of external forces on reaction rates through Arrhenius' law, it does not take into account the cargo or the environment. Recent experiments (see Section 3.4) show that those factors impact the motor dynamics and should not be ignored. In addition, it has been demonstrated that molecular motors, e.g. kinesin, are sensitive to external conditions, like ATP concentration, which change not only the kinetics, but also the whole operating mechanism responsible for mechanical stepping (Guydosh and Block, 2006; Mori et al., 2007). Our approach tries to give a simple physical mechanism behind the force–velocity relation. Below we will elaborate on the model's parameters and highlight the important consequences of the approach described in the previous sections.

3.1. Model parameters

The presented model has two important parameters: x_m, which reflects the motor's ability to deflect forward and backward while following the diffusing cargo, and t_r giving the minimum time needed for chemical and conformational changes between subsequent steps.

x_m: Experiments give us no precise values for the maximum deflection of the kinesin motor (Jeney et al., 2004). This parameter can be related to the protein's elasticity, which appears to play a significant role in the stepping process. After the first experiments on kinesin, it was suggested that the motor stretches the spring-like tether when it makes a step, and that the subsequent elastic relaxation of the tether then pulls the cargo forward (Svoboda et al., 1993).

As shown in Fig. 2C, our model predicts a force–velocity relation for the kinesin-like motor that is almost unaffected by the choice of x_m. The mooring model results in the experimentally observed behavior (i.e. trajectories of the cargo are staircase-like, with position fluctuations between the motor's steps, see Fig. 1 of **SI**). So the stretching of the tether is not the only possible explanation of the experimental outcome.

The weak dependence of the MFPT, and thus of the motor's velocity, on x_m may seem counterintuitive, but a good quantitative explanation can be given (see Section 3 in **SI**).

t_r: The minimum dwell time, t_r, is easier to estimate, at least for a kinesin-like motor. From Refs. Visscher et al. (1999) and Carter and Cross (2005) we take 800 nm/s as the velocity of unloaded kinesin. Knowing the length of a single step, $L=8$ nm, we find $t_r=10$ ms. Even for a fixed t_r, unaffected by external forces, we observe the decrease in the motor's velocity in the presence of high loads. In this regime the duration of the chemical cycle is no longer the limiting factor — it is the diffusion that is affected by the force.

To verify our model we have compared the predicted force–velocity curves with the experimental ones from Visscher et al. (1999) and Carter and Cross (2005), see Fig. 2. One observes that even without taking the backstepping into account our model agrees well with the points from Block et al. (2003) for high ATP concentration. With decreasing ATP concentration the time needed for successful hydrolysis increases and so does t_r. But experiments also show that velocity gets more sensitive to load and starts falling faster at lower ATP concentrations, see Fig. 4A in Block et al. (2003). Our model (Fig. 3B and D), at least in its simple form, cannot explain this increased sensitivity, which to our knowledge has not been widely discussed in the literature (however see Mogilner et al., 2001 for similar observations and insightful discussion).

Another drawback of our approach is associated with the experimental observation that the stall force increases with ATP concentration (Block et al., 2003). The mooring model predicts that the stall force is almost unaffected by the changes of t_r, as shown in Fig. 3.

We put forth that an explanation might be found in the different ways in which the motor apparently waits for the succeeding chemical transitions under different ATP concentrations. Using FRET, Mori et al. observed that the two-head-bound state predominates for high ATP concentrations (Mori et al., 2007). When there is less chemical fuel in the buffer, kinesin waits for the completion of its chemo-mechanical cycle in a one-head-bound state. It is possible that in the one-head-bound state the strain generated by the load affects the motor differently than in a two-head-bound state.

Another relevant observation is that the speed of an unloaded kinesin differs significantly between Block et al. (2003) and Carter and Cross (2005). Additionally, the motors used by those groups show different backstepping patterns (see *Backstepping*). This striking discrepancy between the results from Block et al. (2003) and Carter and Cross (2005) may be, at least to some extent, explained by the difference between the proteins. While Block et al. used kinesin purified from the squid optic lobe, Carter and Cross used kinesin from *Drosophila melanogaster*. Also, the origins of the microtubules as well as the experimental assays and procedures were slightly different. It is a commonly held view that dynein motors taken from different organisms exhibit different features (see Reck-Peterson et al., 2012 for a review), while kinesins are homogeneous between species. But that view may not be entirely accurate.

In our analysis we did not consider the time of the conformational transition responsible for the step (i.e. moving the rear head to in front of the leading head). Carter and Cross found that the mechanical component of a step takes around 15 μs for kinesin-1 transporting a 0.5 μm bead (Carter and Cross, 2005). This is a negligible amount of time compared to the duration of the entire cycle.

We note that it may be possible to change the times for the different transitions in mutants. An elongated neck linker may, for instance, hinder the docking of the free head and lead to a larger t_r (Yildiz et al., 2008).

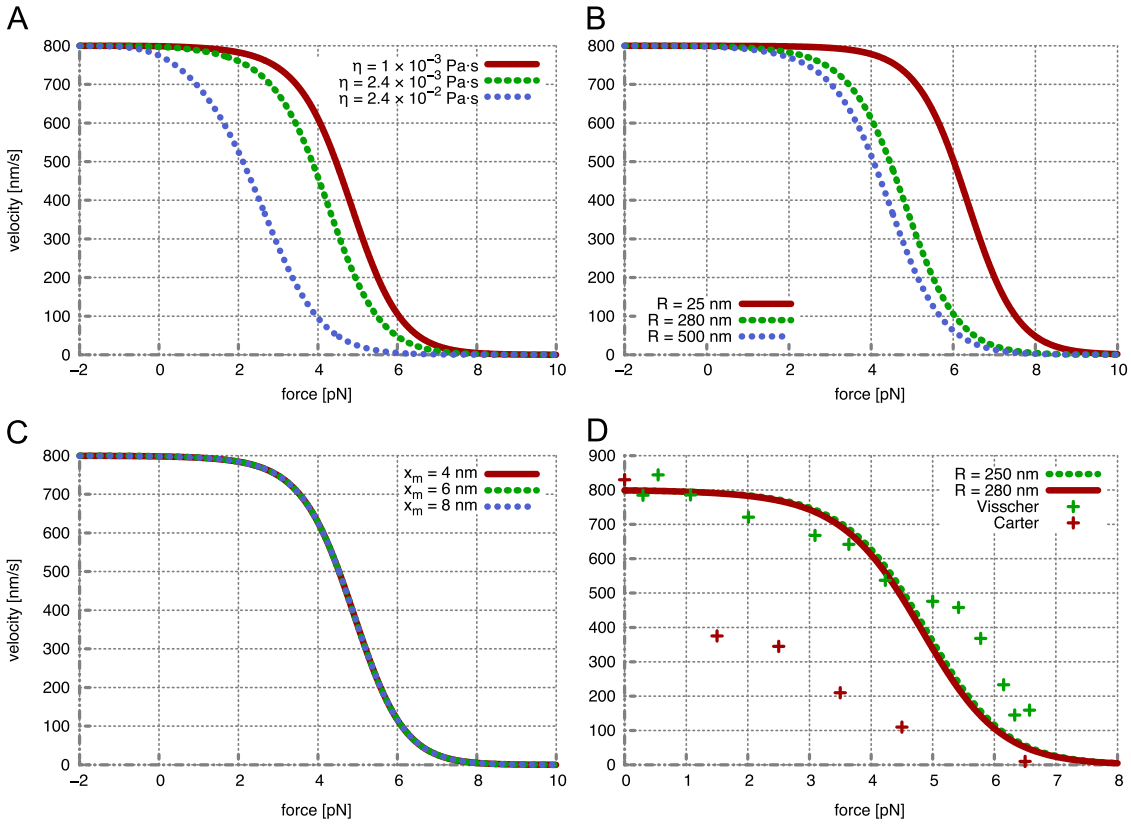

Fig. 2. *Force–velocity curve for a kinesin-like motor without backsteps.* Different values of the buffer's viscosity (η), the cargo radius (R), and x_m range size are used. Note that γ and R enter the dynamics of Eq. (1) through $\gamma = 6\pi\eta R$ and $D = k_B T/\gamma$. The results are compared with experimental data. (A) For a given force, the transport is faster for smaller viscosities. R=280 nm, x_m=8 nm, t_r=10 ms and L=8 nm. (B) For a given force, the transport is faster for smaller cargos. $\eta = 1 \times 10^{-3}$ Pa s, x_m=8 nm, t_r=10 ms and L=8 nm. (C) Changing x_m appears to have negligible effect on the force–velocity relation. $\eta = 1 \times 10^{-3}$ Pa s, R=250 nm, t_r=10 ms and L=8 nm. (D) Experimental data from Visscher et al. (1999) (green) and Carter and Cross (2005) (red). $\eta = 1 \times 10^{-3}$ Pa s, t_r=10 ms, x_m=8 nm and L=8 nm. (For interpretation of the references to color in this figure caption, the reader is referred to the web version of this paper.)

3.2. Backstepping

The motion of a processive molecular motor is highly directed. However, sometimes the motor takes a step in the backward direction. For kinesin-1, backsteps are steps toward the microtubule's minus end. Visscher et al. found – and Block et al. later confirmed – five to ten backsteps for every 100 forward steps (Visscher et al., 1999; Block et al., 2003). This result appeared load independent. In a more recent study Carter and Cross found about one backstep for every 802 forward steps when no load was applied (Carter and Cross, 2005). With an increasing load, the backstep fraction was found to increase rapidly, but the forward-to-backward step ratio turned out to be independent of the ATP concentration (Carter and Cross, 2005). For large loads, backsteps constitute a significant fraction of the total number of steps. This fraction approaches unity for the stall force and falls below unity for higher loads. Therefore, neglecting the backsteps is no longer legitimate for high loads. Below we show how to implement backsteps into the mooring model.

We start by introducing new variables, listed in Table 2.

It is easy to see that

$$\frac{v}{L} = \frac{n_F - n_B}{\sum_{i=1}^{n_F} t_F^{(i)}(F) + \sum_{j=1}^{n_B} t_B^{(j)}(F)} \approx \frac{p_F - p_B}{p_F\langle t_F(F)\rangle + p_B\langle t_B(F)\rangle}$$

$$= \frac{1-2p_B}{\langle t_F(F)\rangle + p_B(\langle t_F(-F)\rangle - \langle t_F(F)\rangle)}. \tag{14}$$

Combining formulas (11) and (14) we arrive at the result:

$$v = \frac{1-2p_B}{Fzt_r + \left(\dfrac{e^{zx_m}}{\sinh zx_m} - 2p_B\right)(\sinh zL - zL)} FLz. \tag{15}$$

The last step in the derivation is to substitute a phenomenological relationship between the backstep probability p_B and the other model parameters. To check our model we have used two datasets, one from Block et al. (2003), with constant p_B, and the other from Carter and Cross (2005). In the latter reference Carter and Cross found a logistic curve that links p_B with the load force F:

$$p_B = \frac{1}{1 + ae^{-bF}}, \tag{16}$$

with a=802 and b=0.95 and the load F given in pN (Carter and Cross, 2005). The results for those two schemas of backstepping are presented in Fig. 3(A,B) and (C,D), respectively.

3.3. Viscosity and cargo dimension

Most of the molecular motor experiments are conducted *in vitro*, i.e. in some buffer solution of a homogeneous viscosity. In this study we examine motion in different homogeneous solutions — water, buffer solution, and a reference solution (Fig. 2A). For the buffer we took the effective viscosity $\eta = 2.4 \times 10^{-3}$ Pa s, as in Beausang et al. (2007). The nearby presence of a wall may lead to the motor and cargo construct "feeling" a higher viscosity. Also the nearby presence of the

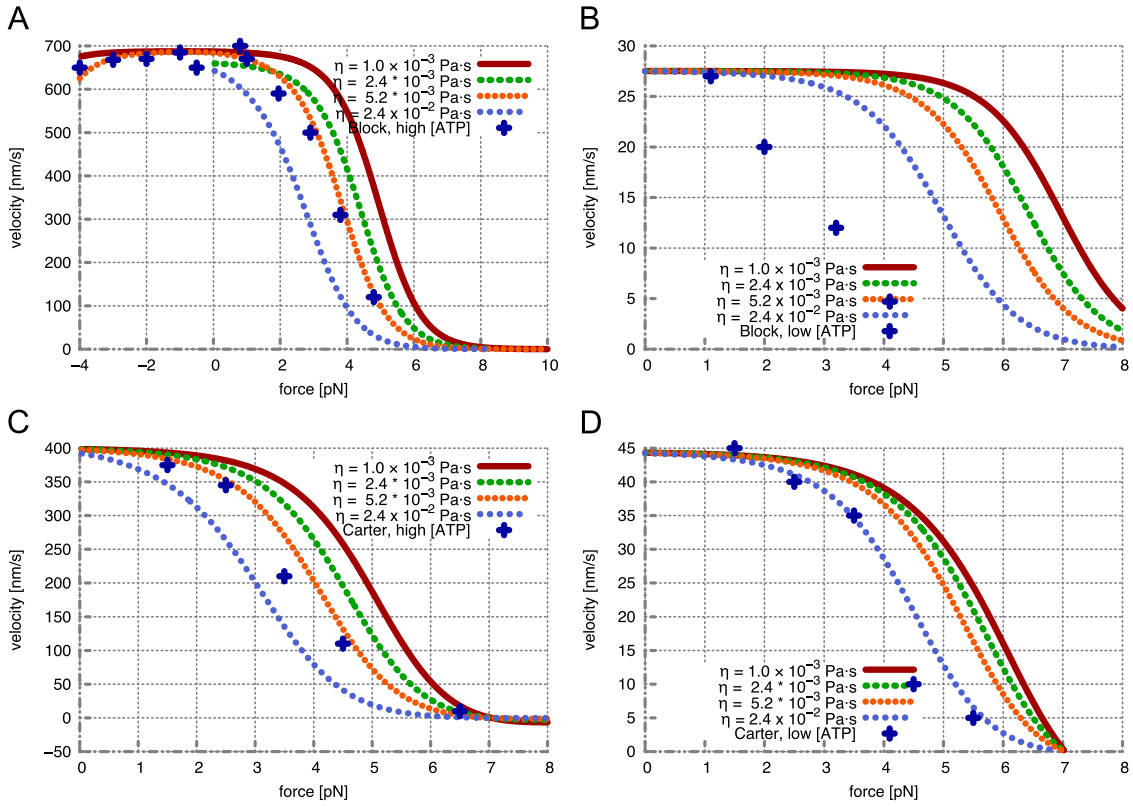

Fig. 3. *Force–velocity curves for a backstepping kinesin-like motor.* Different values of the buffer's viscosity and different t_r, reflecting different ATP concentrations, are used. Two different implementations were used: one with a constant ratio of forward-to-backward steps (panels A and B) and one with an exponential relation between that ratio and applied external force (panels C and D), see section Backstepping. (A) $R=250$ nm, $x_m=8$ nm, $t_r=10$ ms, $p_B=0.07$ and $L=8$ nm. (B) $R=250$ nm, $x_m=8$ nm, $t_r=250$ ms, $p_B=0.07$ and $L=8$ nm. (C) $R=280$ nm, $x_m=8$ nm, $t_r=20$ ms, $p_B=1/(1+802e^{-0.95F})$ and $L=8$ nm. (D) $R=280$ nm, $x_m=8$ nm, $t_r=180$ ms, $p_B=1/(1+802e^{-0.95F})$ and $L=8$ nm. Experimental data are from Block et al. (2003) and Carter and Cross (2005) for panels A–B and C–D, respectively.

Table 2
Variables used for describing backstepping.

$p_{F(B)}$	Probability of taking a forward (backward) step; it can be a function of load or a constant
$n_{F(B)}(F)$	Number of forward (backward) steps
$t_{F(B)}(F)$	Random variable describing a duration of forward (backward) step under load F
v	Velocity; a random variable approaching with probability one its mean value in $n\to\infty$ limit

motor may cause the cargo to "feel" a higher effective viscosity. So the third solution we used is a hypothetical environment with a viscosity 10 times higher than the aforementioned $\eta = 2.4 \times 10^{-3}$ Pa s of the buffer solution. Results depicted in Fig. 2A show the sensitivity of the velocity to the viscosity. As a general rule, with the same motor, the cargo's motion slows down as viscosity increases. Since the drag coefficient γ depends linearly on viscosity η, higher η implies smaller D, i.e. smaller Brownian kicks felt by the cargo. As a consequence, the dwell times in one position are longer — it takes a longer time to reach another no-return point. Also the stall force decreases significantly for higher viscosities. The decrease of the amplitude of the thermal noise makes the cargo less mobile as at the same time the effective force, F/γ (cf. Eq. (1)), also decreases.

Interestingly, mooring-model predictions can be fitted to the experimental data even better by increasing the viscosity of the buffer tenfold (Fig. 3 and Fig. 2 in **SI**). Even the non-monotonic shape of the force–velocity curve for assisting loads, reported by Block et al. (2003), can be reproduced for a viscosity of $\eta = 5.2 \times 10^{-3}$ Pa s, cf. Fig. 2 in **SI**. Hence, the question about the microscopic velocity "felt" by the diffusing cargo in an *in vitro* motility experiment arises. There is empirical evidence suggesting that the *in vivo* effective viscosity is a function of the probe's size: the bigger the difference in size between crowding agents and the probe, the less viscous the environment (Kalwarczyk et al., 2011; Ochab-Marcinek and Holyst, 2011). It is tempting to use a higher "effective" viscosity when comparing the theoretical predictions of the mooring model with experiments. Without going into further detail we conclude at this point that the environment is very important for motor-driven motility. It is regrettable that many experimental reports on motor-protein motion do not include the value of the medium's viscosity.

The same relation as between viscosity and velocity is observed for cargo size and velocity. As our base cargo's radius size we have used $R=250$ nm, which corresponds with the size of the beads used by Carter and Cross (2005). Additionally, we have also analyzed motor–cargo dynamics for smaller ($R=25$ nm) and bigger ($R=500$ nm) cargos, see Fig. 2B. With $\gamma = 6\pi\eta R$ it is obvious that the drag is larger for larger beads. The diffusion coefficient $D = k_B T/\gamma$ is smaller for larger beads.

Cargo size and viscosity appear to strongly affect the force–velocity characteristics. These results suggest that it is important to consider viscosity and cargo size when interpreting experimental outcomes.

3.4. Comparison with experimental data

In this section we present some experimental findings, taken from the literature, that show how data involving the environment's viscosity, cargo size, and the structure-function connection support the mooring model.

As early as in 1994 Hunt et al. (1994) reported in a very elegant paper that the motion of microtubules propelled by single kinesin molecules for gliding assay experiments depends on both the viscosity of the buffer and the microtubule length. That is also what our mooring model would predict, since it is perfectly applicable for gliding assays experiments as well as for bead-pulling against an external force (cf. Fig. 3 in **SI**).

After analyzing four possible mechanisms of motor action, the authors excluded a "filament-diffusion model" that was somewhat similar to our cargo-mooring model. Their filament-diffusion model predicted a speed in high viscosity solutions that was smaller than the one observed experimentally. Hunt et al. also showed that the microtubule is unable to diffuse in a viscous solution through $L=8$ nm during the time in which kinesin takes its mechanical step ($t<72$ μs in their paper).

Whereas in the "filament-diffusion model" the diffusion and the chemical changes are separate stages, in the mooring mechanism the cargo diffuses for the entire time needed to complete the chemical cycle of ATP hydrolysis and ADP-P_i release. That time sums up to around 10 ms for all the chemical transitions. The mechanical step takes only μs for an unloaded kinesin motor (Carter and Cross, 2005). This assumption of our mooring model is consistent with what experimentally obtained trajectories show: Brownian motion of the cargo is observed between steps and not only during them. Within 10 ms, the diffusing cargo (or, as in Hunt et al., 1994, microtubule, cf. Fig. 3 in **SI**) can easily cover the distance $L=8$ nm needed to trigger the step when no external force is applied. This results in different predictions of the two models.

For the filament-diffusion model of Ref. Hunt et al. (1994), the velocity diverges with decreasing viscosity. In our mooring model the velocity of the motor saturates as the viscosity goes down. This is because the time of one step cannot be shorter than the time of the reaction cycle (t_r) plus the time of the mechanical transition.

Another difference is the estimation of the maximum force a motor can sustain, i.e., stall force. Hunt et al. show that for the filament-diffusion model this is $2k_bT/L\approx 1pN$. This is less than experimental observations and our theoretical predictions. This is again because of the filament-diffusion model's assumption that the diffusive motion of the cargo takes only a fraction of the hydrolysis time t_r. Our mooring model, built on experimental observations, predicts that the stall force, even for highly viscous buffer, is much higher than the one predicted by the filament diffusion model, see Figs. 2 and 3.

Very recently Efremov et al. reported a series of *in vivo* experiments that reveal a dependence of the kinesin-based transport on the size of the cargo (Efremov et al., 2014). The velocity of peroxisomes moved by multiple kinesins decreases when these peroxisomes are getting bigger. Interestingly, this is not so obvious for myosin Va. One explanation may be that myosin exhibits complex behavior while interacting with rather disordered actin filaments. Myosin Va can take steps of different lengths while cross-linking between different tracks. This makes observations as well as data analysis problematic. Nevertheless, the observed cargo-size dependence for kinesin-powered peroxisome motion is an important empirical fact that is accounted for by the mechanism that we propose.

The most essential assumption of the mooring mechanism is that there is a kind of communication between the top end of the stalk and, through its bottom end, neck linkers and motor domains. In other words, the deflection of the stalk is assumed to generate a "signal" — i.e. mechanical strain — which can trigger or prevent the motor's stepping. Yildiz et al. (2008) studied the behavior of kinesins with extended neck linkers. They observed that the velocity of such a modified motor is decreasing with growing length of the artificial amino acid inset. What is even more important, by applying assisting loads with an optical tweezer, the authors were able to speed up the modified motors. They could also trigger steps with a forward load in the absence of ATP. Pulling (that is, deflecting the stalk towards the plus end of the microtubule) alone can make kinesin walk in its natural step-by-step manner! These results prove that the position of the cargo, manifested by the stalk's deflection, is important for the processive motion of the motor.

4. Discussion

Kinesin molecular motors, taking care of intracellular transport needs of eukaryotic cells, are among the best known proteins. The energy-consuming active transport in which they are involved is thought to be an evolutionary improvement over free diffusion, the latter being just not sufficiently efficient, fast and reliable for cells bigger than 1 μm. However, since our knowledge about kinesins comes mainly from *in vitro* experiments, we are still far from understanding all the factors that impact their behavior *in vivo*.

Kinesin hydrolyzes one ATP molecule per step. But how the energy is transduced into effective work is still the subject of much debate, experimentation and modeling. The experimental trajectories show that the position of the bead fluctuates around a fixed position and eventually makes a 8 nm jump (in the case of kinesin) to the next fixed position, around which it will again fluctuate for some time. This results in a "staircase"-like trajectory as in Svoboda et al. (1993) (cf. Fig. 1 in **SI**).

Conceiving of the motor as diffusing along an abstract reaction coordinate in a chemical space does not lead to any insight about what is really happening with the motor and its cargo. In the mechanical reality it is the cargo that diffuses in a real physical space while the motor stays attached to the microtubule. Since the analytical results obtained under the assumptions of the proposed cargo-mooring mechanism correspond quite well with experimental data, we suggest that, when studying the intracellular active transport, it is necessary to concentrate not only on the motor, but also on the entire motor–cargo–environment system. This is because the viscosity of the environment and the cargo's size are seen to significantly affect the motor's dynamics.

In vivo kinesin transports vesicles of about 50 nm in diameter. The stalk that connects the motor and the vesicle has a length of about 100 nm. Vesicle and/or stalk can get entangled in the cytoskeletal network. Kinesin that "gets stuck" in such a way will more easily detach from the biopolymer that it is walking on. It is well known that under high loads the detachment rate of a kinesin motor increases (Jamison et al., 2010). There are even more evident clues for the regulatory function of the stalk. By changing the accessibility of the nucleotide pocket on kinesin's heads, the stalk modulates the dynamics of the entire motor protein (Dietrich et al., 2008; Wong et al., 2009). This means that there is a possibility of "communication" between the cargo and the motor — communication that occurs via the stalk.

If the motor "feels" the impact of diffusive motion on a cargo, the generated strain may slow down or speed up chemical transitions (e.g. the release of ADP) that drive the motility. For example, the catalytic cycle could be accelerated if the cargo can more easily find a free space

to diffuse a little bit closer towards the microtubule's plus end and thus trigger a next step. This idea gives a possible explanation of the Arrhenius-like dependency of kinesin's dynamics under load. In *in vitro* experiments the external force is applied on the cargo, so it is the cargo's diffusive motion that is affected directly. Since the information about the actual position of the cargo is transmitted to the motor protein via the stalk and since the orientation of the stalk (i.e. its deflection) modulates the chemical transitions in the motor domains, our proposed mooring model is plausible from a structural point of view.

The important role of thermal motion seems universal for many intracellular processes. Already in 1993 Peskin et al. showed how growing polymers may generate forces by rectifying Brownian fluctuations (Peskin et al., 1993). In our model, which actually is a version of the Brownian ratchet, the motor is effectively rectifying the Brownian motion of the cargo to which it is tethered. It is this rectification that requires the chemical energy from ATP hydrolysis. No real “pulling” occurs.

What makes our model different from typical ratchet models is the role it gives to the cargo. We no longer consider the diffusion of a single motor in an abstract chemical space. Instead, we consider the diffusion of a real cargo in a real laboratory space.

A future goal would be to present a more detailed model of the mooring mechanism. It should be extended to describe the action of other cytoskeletal motor proteins: dynein and myosin. Kinesin and dynein are structurally very different. The latter may take not only single 8 nm steps, but also double (16 nm) and triple (24 nm) ones (Reck-Peterson et al., 2012, 2006; Gennerich et al., 2007). Dynein is also load-sensitive, but in a different way than kinesin (Rai et al., 2013). Yet it appears that dynein is like kinesin in that it has also evolved a coordinating activity in the stalk (Ori-McKenney et al., 2010).

The collective behavior of several motors carrying one cargo should also be examined.

Summarizing, what we propose is an ability of kinesins, and possibly other types of motors as well, to wait for the cargo to diffuse sufficiently far before they take an actual step. Our suggestion is a more extensive role for the stalk. Strain on the stalk will not merely be a signal for detachment. It can also trigger a next step.

Acknowledgments

We would like to thank Ewa Gudowska-Nowak, Anna Ochab-Marcinek, Zenon Rajfur and Michał Świątek for beneficial discussions. The project has been supported by the European Science Foundation within the program EPSD (Exploring Physics of Small Devices). B.L. wishes to thank the Foundation for Polish Science (International Ph.D. Projects Program co-financed by the European Regional Development Fund covering, under the Agreement no. MPD/2009/6; the Jagiellonian University International Ph.D. Studies in Physics of Complex Systems) and Jagiellonian University Institute of Physics for a donation DSC K/DSC/001586.

Appendix A. Supplementary data

Supplementary data associated with this paper can be found in the online version at http://dx.doi.org/10.1016/j.jtbi.2015.03.007.

References

Asbury, C.L., 2003. Kinesin moves by an asymmetric hand-over-hand mechanism. Science 302 (5653), 2130–2134.
Astumian, R.D., 1997. Thermodynamics and kinetics of a Brownian motor. Science 276 (5314), 917–922.
Astumian, R., Bier, M., 1994. Fluctuation driven ratchets: molecular motors. Phys. Rev. Lett. 72 (11), 1766–1769.
Beausang, J.F., Zurla, C., Finzi, L., Sullivan, L., Nelson, P.C., 2007. Elementary simulation of tethered Brownian motion. Am. J. Phys. 75 (6), 520.
Bier, M., Derényi, I., Kostur, M., Astumian, R., 1999. Intrawell relaxation of overdamped Brownian particles. Phys. Rev. E 59 (6), 6422–6432.
Block, S.M., 2007. Kinesin motor mechanics: binding, stepping, tracking, gating, and limping. Biophys. J. 92 (9), 2986–2995.
Block, S.M., Absury, C.L., Shaevitz, J.W., Lang, M.J., 2003. Probing the kinesin reaction cycle with a 2D optical force clamp. Proc. Natl. Acad. Sci. 100 (5), 2351–2356.
Carter, N.J., Cross, R.A., 2005. Mechanics of the kinesin step. Nature 435 (7040), 308–312.
Clancy, B.E., Behnke-Parks, W.M., Andreasson, J.O.L., Rosenfeld, S.S., Block, S.M., 2011. A universal pathway for kinesin stepping. Nat. Struct. Mol. Biol. 18 (9), 1020–1027.
Dietrich, K.A., Sindelar, C.V., Brewer, P.D., Downing, K.H., Cremo, C.R., Rice, S.E., 2008. The kinesin-1 motor protein is regulated by a direct interaction of its head and tail. Proc. Natl. Acad. Sci. 105 (26), 8938–8943.
Efremov, A.K., Radhakrishnan, A., Tsao, D.S., Bookwalter, C.S., Trybus, K.M., Diehl, M.R., Delineating cooperative responses of processive motors in living cells, Proc. Natl. Acad. Sci. Early Edition (26) (2014) 8938–8943.
Fisher, M.E., Kolomeisky, A.B., 1999. The force exerted by a molecular motor. Proc. Natl. Acad. Sci. 96 (12), 6597–6602.
Gardiner, C.W., 1997. Handbook of Stochastic Methods: for Physics, Chemistry and the Natural Sciences. Springer Series in Synergetics, 2nd ed., Springer, Berlin.
Gennerich, A., Carter, A.P., Reck-Peterson, S.L., Vale, R.D., 2007. Force-induced bidirectional stepping of cytoplasmic dynein. Cell 131 (5), 952–965.
Guydosh, N.R., Block, S.M., 2006. Backsteps induced by nucleotide analogs suggest the front head of kinesin is gated by strain. Proc. Natl. Acad. Sci. 103 (21), 8054–8059.
Howard, J., 1997. Molecular motors: structural adaptations to cellular functions. Nature 389 (6651), 561–567.
Howard, J, 2001. Mechanics of Motor Proteins & the Cytoskeleton. Sinauer Associates Incorporated.
Hunt, A.J., Gittes, F., Howard, J., 1994. The force exerted by a single kinesin molecule against a viscous load. Biophys. J. 67 (6651), 766–781.
Jamison, D.K., Driver, J.W., Rogers, A.R., Constantinou, P.E., Diehl, M.R., 2010. Two Kinesins transport Cargo primarily via the action of one motor: implications for intracellular transport. Biophys. J. 99 (9), 2967–2977.
Jeney, S., Stelzer, E.H.K., Grubmüller, H., Florin, E.-L., 2004. Mechanical properties of single motor molecules studied by three-dimensional thermal force probing in optical tweezers. ChemPhysChem 5 (8), 1150–1158.
Jülicher, F., Ajdari, A., Prost, J., 1997. Modeling molecular motors. Rev. Mod. Phys. 69 (4), 1269–1282.
Kalwarczyk, T., Ziebacz, N., Bielejewska, A., Zaboklicka, E., Koynov, K., Szymański, J., Wilk, A., Patkowski, A., Gapiński, J., Butt, H.-J., Holyst, R., 2011. Comparative analysis of viscosity of complex liquids and cytoplasm of mammalian cells at the nanoscale. Nano Lett. 11 (5), 2157–2163.
Kozielski, F., Sack, S., Marx, A., Thormählen, M., Schönbrunn, E., Biou, V., Thompson, A., Mandelkow, E.M., Mandelkow, E., 1997. The crystal structure of dimeric kinesin and implications for microtubule-dependent motility. Cell 91 (7), 985–994.
Liepelt, S., Lipowsky, R., 2007. Kinesin's network of chemomechanical motor cycles. Phys. Rev. Lett. 98 (25), 258102.
Mogilner, A., Fisher, A.J., Baskin, R.J., 2001. Structural changes in the neck linker of kinesin explain the load dependence of the motor:s mechanical cycle. J. Theor. Biol. 211 (2), 143–157.
Mori, T., Vale, R.D., Tomishige, M., 2007. How kinesin waits between steps. Nature 450 (7170), 750–754.
Ochab-Marcinek, A., Holyst, R., 2011. Scale-dependent diffusion of spheres in solutions of flexible and rigid polymers: mean square displacement and autocorrelation function for FCS and DLS measurements. Soft Matter 7, 7366–7374.
Ori-McKenney, K.M., Xu, J., Gross, S.P., Vallee, R.B., 2010. A cytoplasmic dynein tail mutation impairs motor processivity. Nat. Cell Biol. 12 (12), 1228–1234.
Peskin, C.S., Odell, G.M., Oster, G.F., 1993. Cellular motions and thermal fluctuations: the Brownian ratchet. Biophys. J. 65 (1), 316–324.
Rai, A.K., Rai, A., Ramaiya, A.J., Jha, R., Mallik, R., 2013. Molecular adaptations allow dynein to generate large collective forces inside cells. Cell 152 (1–2), 172–182.
Reck-Peterson, S.L., Yildiz, A., Carter, A.P., Gennerich, A., Zhang, N., Vale, R.D., 2006. Single-molecule analysis of dynein processivity and stepping behavior. Cell 126 (2), 335–348.
Reck-Peterson, S.L., Vale, R.D., Gennerich, A., 2012. Motile properties of cytoplasmic dynein. In: Hirose, K., Amos, L.A. (Eds.), Handbook of Dynein. Pan Stanford Publishing Pte. Ltd, pp. 145–172.
Schilstra, M.J., Martin, S.R., 2006. An elastically tethered viscous load imposes a regular gait on the motion of myosin-V. Simulation of the effect of transient force relaxation on a stochastic process. J. R. Soc. Interface, http://dx.doi.org/10.1098/rsif.2005.0098.
Shastry, S., Hancock, W.O., 2011. Interhead tension determines processivity across diverse N-terminal kinesins. Proc. Natl. Acad. Sci. 108 (39), 16253–16258.
Svoboda, K., Schmidt, C.F., Schnapp, B.J., Block, S.M., 1993. Direct observation of kinesin stepping by optical trapping interferometry. Nature 365 (6448), 721–727.
Tomishige, M., Stuurman, N., Vale, R.D., 2006. Single-molecule observations of neck linker conformational changes in the kinesin motor protein. Nat. Struct. Mol. Biol. 13 (10), 887–894.
Visscher, K., Schnitzer, M.J., Block, S.M., 1999. Single kinesin molecules studied with a molecular force clamp. Nature 400 (6740), 184–189.

Wong, Y.L., Dietrich, K.A., Naber, N., Cooke, R., Rice, S.E., 2009. The kinesin-1 tail conformationally restricts the nucleotide pocket. Biophys. J. 96 (7), 2799–2807.
Yildiz, A., Tomishige, M., Vale, R.D., Selvin, P.R., 2004. Kinesin walks hand-over-hand. Science 303 (5658), 676–678.
Yildiz, A., Tomishige, M., Gennerich, A., Vale, R.D., 2008. Intramolecular strain coordinates kinesin stepping behavior along microtubules. Cell 134 (6), 1030–1041.